Available online at www.sciencedirect.com

ScienceDirect

Ceramics International 40 (2014) 1199–1204

CERAMICS INTERNATIONAL

www.elsevier.com/locate/ceramint

Short communication

Microstructure analysis of C_f/SiC–ZrC composites in both fabrication and plasma wind tunnel testing processes

Q. Feng[a], Z. Wang[b,c,*], H.J. Zhou[b,c], P. He[b,c], L. Gao[b,c], Y.M. Kan[b,c], X.Y. Zhang[b,c], Y.S. Ding[b,c], Shaoming Dong[b,c]

[a]*Analysis and Testing Center, Donghua University, Shanghai 201620, China*

[b]*State Key Laboratory of High Performance Ceramics and Superfine Microstructure, Shanghai Institute of Ceramics, Shanghai 200050, PR China*

[c]*Structural Ceramics and Composites Engineering Research Center, Shanghai Institute of Ceramics Chinese Academy of Sciences, Shanghai 200050, PR China*

Received 17 February 2013; received in revised form 25 May 2013; accepted 27 May 2013
Available online 6 June 2013

Abstract

Two kinds of C/SiC–ZrC composites were fabricated through different methods in this study. For composite S, ZrC was just incorporated through the impregnation of slurry containing ZrC particles. For the other composite S*, infiltration and pyrolysis of the ethanol dissolvable polyzirconoxanesal (PSZ) was performed and some more ZrC was synthesized via in-situ carbothermal reduction reaction between PSZ derived ZrO_2 and carbon. Scanning electron microscopy (SEM) was applied to characterize the distribution of ZrC, the morphology of composite fracture surface as well as the ablated surface of composite S*. Based on the SEM analysis results, the microstructure evolution as well as the ablation behavior of C/SiC–ZrC composites was discussed.

Keywords: B. Composite; B. Electron Microscopy; C/SiC–ZrC

1. Introduction

The search for high temperature structural materials has been driven by the development of three technologies: rocket propulsion systems, atmospheric re-entry vehicles and hypersonic flight vehicles. The current space shuttle orbiter has a blunt body design which limits the maximum surface temperature on the leading edges of the orbiter to ~1650 °C. By employing blunt leading edge design the lift-to-drag ratio can be lowered, thereby reduce the maneuverability and cross-range for the vehicle during atmosphere re-entry. However, the application of sharp leading edges for new hypersonic aircraft will lead to a great increase of temperature at the surface of components. The surface temperature of component is believed to be proportional to the inverse square root of the body radius. Therefore, materials for sharp leading edges should withstand oxidizing atmospheres at higher temperatures.

Some efforts have been contributed to develop high reliable materials which can sustain oxidizing environments at ultra high temperatures. Ultra-high temperature ceramics (UHTCs) based on the carbides, nitrides and borides of group IV_B and V_B transition metals have received considerable attention, due to the combination of advantages such as high melting temperature, high thermal conductivity and excellent oxidation resistance at high temperatures. However, the low fracture toughness and poor thermal shock resistance of UHTCs have become issues for their application as high temperature components. In order to develop ultra high temperature materials with higher reliability, some attempts have been made to develop fiber reinforced UHTC-based matrix composites. Yang [1,2] tried to develop ZrB_2–SiC-based composites by incorporating short carbon fibers as reinforcements. Composites with a fiber volume fraction of about 20% were fabricated through the conventional hot-pressing method. The fracture toughness increased from 4.3 MPa $m^{1/2}$ to 6.6 MPa $m^{1/2}$, which is still relatively low when compared to continuous fiber reinforced ceramic matrix composites. It is believed that the fracture toughness can be obviously improved by applying continuous fibers as

*Corresponding author at: 1295 Dingxi Road, Shanghai 200050, PR China. Tel.: +86 21 5241 4230; fax: +86 21 5241 3903.
E-mail address: jeff@mail.sic.ac.cn (Z. Wang).

0272-8842/$ - see front matter © 2013 Elsevier Ltd and Techna Group S.r.l. All rights reserved.
http://dx.doi.org/10.1016/j.ceramint.2013.05.097

reinforcements. However, with the incorporation of fiber reinforcements, some new problems such as the need for new processing approaches, oxidation of the reinforcing phase as well as the thermal expansion mismatch between carbon fibers and the UHTC matrix should be considered. Consequently, much effort has been devoted to overcome the afore-mentioned problems. The choice of fiber reinforcements for UHTCs was limited to carbon fibers for the consideration of thermal stability and strength at ultra high temperatures. In the past several years, fabrication of UHTC-based composites and evaluation of their ablation behavior have become a hotspot. Several methods have been applied to introduce UHTC phases into the matrix of composites, such as slurry impregnation [3–6] or slurry paste [7], organic precursor infiltration and conversion [8–11], reactive melt infiltration [12–16] and chemical vapor infiltration [17].

To overcome the problems of low content and inhomogeneous distribution of UHTC phases accompanied in the slurry impregnation process, ZrC was introduced into the matrix of composites through polymer infiltration and in-situ synthesis. In this paper, the microstructure and ablation behaviors of as-fabricated C/SiC–ZrC composites were studied. The mechanism for ablation enhancement has been discussed based on the microstructures of composites before and after plasma wind tunnel testing.

2. Experimental procedure

Firstly, carbon fiber weftless plies and short-cut-fiber webs (T700, 12K, Toray, Japan) were stacked alternatively followed by a needle-punching process to form 3D needle-punched fiber preforms. The fiber fraction is about 30% and the structure of 3D needle-punched fiber preforms is shown in Fig. 1. Afterward, the preforms were coated with 100 nm/50 nm PyC/SiC interphase by CVI. The source gas for PyC is ethene and those for SiC were H_2 and methylchlorosilane (MTS) with the molar ratio of H_2 to MTS is 10. The deposition conditions for both PyC interphase and SiC interphase were 3 kPa and 1050 °C. Homogeneous slurry was prepared by ball-milling ZrC powders (Kai'er Nanometer Technology Development Co. Ltd., Hefei, China) and phenolic resin with a weight ratio of 70:30, using ethanol as solvent. Then the coated carbon fiber preforms were impregnated in afore-mentioned slurries and pyrolysed at 900 °C for 30 min to convert phenolic resin into carbon. Then some composites were densified through polymer infiltration and pyrolysis (PIP) process using polycarbosilane (PCS) as precursor, denoted as composites S. The pyrolysis conditions for PCS were 1100 °C and 30 min. For other composites, polyzirconoxanesal (PSZ) described elsewhere [18] was applied as precursor for conversion of ZrC. 6 cycles of infiltration and pyrolysis of PSZ were carried out with the pyrolysis temperature of 900 °C and the pyrolysis time of 30 min, then the samples were heat-treated at 1600 °C for 1.5 h to convert the derived ZrO_2 and carbon into ZrC. After that the composites were further densified through 6 cycles of PIP using polycarbosilane (PCS) as precursor. These composites were denoted as composites S*.

C/SiC–ZrC composites fabricated through different processes were cut into bars along 0° weftless fibers for 3-point-bending test. Composite S* was cut and ground into 50 mm × 25 mm × 5 mm specimens for plasma wind tunnel testing, as shown in Fig. 2. During testing, a nitrogen/oxygen mixture gas (80/20) flowing at a high velocity of about 1000 m/s was used to simulate the testing environment, while the sample was assembled at a 45° angle to the gas flow with a 10 mm distance from the nozzle exit and the samples were tested for 300 s. The flame temperature was calculated to be 2500 K according to the heating current.

Microstructure and composition analyses were performed by scanning electron microscopy (SEM) and energy dispersive X-ray micro-analyzer (EDX) on the polished cross-sections, fracture surface as well as the as-exposed surfaces. A thin platinum coating was cast on the polished piece to increase the electrical conductivity and prevent electrostatic charging during SEM observations.

Fig. 2. Plasma wind tunnel testing of C/SiC–ZrC composites.

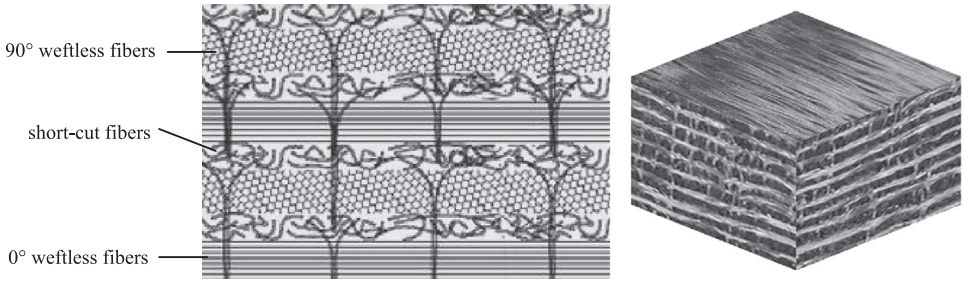

Fig. 1. Structure of 3D needle-punched fiber preform.

3. Results and discussions

Fig. 3 shows that though ZrC powders were claimed by the manufacturer to be in the size of nanoscale, aggregates with a size of about 1 μm are present in the powder.

Fig. 4 shows the micrographs of C/SiC–ZrC composites fabricated through different processes. It can be concluded that only small amount of ZrC particles (with bright contrast due to the containing of heavier element Zr) can be introduced into composites through slurry impregnation (Fig. 4a). ZrC phases mainly distribute in the inter-bundle matrix zones, almost no ZrC is present in the intra-bundle matrix. In the fiber preform fabrication process, needle-technique was applied to integrate carbon fibers in different layers, the pores with size of several hundred micrometers introduced will favor the flow of slurry into the preform. It can be noticed that there are a large amount of carbon fibers in each bundle and the gaps between carbon fibers in the intra-bundle matrix is only several micrometers, which is very near to size of ZrC particles. Therefore, in the slurry impregnation process, when the slurry flowed into the large pores in the preform, the particles on the outer surface of fiber bundles will clog the intra-bundle pores and prevent further particle ingress. Consequently, the intra-bundle zone pores were mainly filled with phenolic resin and ethanol. In the followed PIP densification process, the pores in composite S is filled with PCS-derived SiC and this can amount for the high ZrC content in inter-bundle matrix. Microstructure observation (Fig. 4b) of composite S* reveals that some micro-pores are present in the short-cut-fiber layers. This may be ascribed to the lower fiber fraction and higher porosity present in the short-cut-fiber layers compared to continuous weftless fiber layer, as shown in Fig. 1. In the densification process, the matrix prefers to form around the fibers and it is very difficult to fully fill these large pores in short-cut-fiber layer. Compared to composite S, the fraction and the distribution homogeneity of ZrC in the matrix composite S* were greatly increased (Fig. 4c). In the fabrication process of composite S*, beside from slurry impregnation, PSZ is another approach for ZrC introduction. As PSZ solution has excellent flowability, it can fill almost all pores left both in intra-bundle and inter-bundle

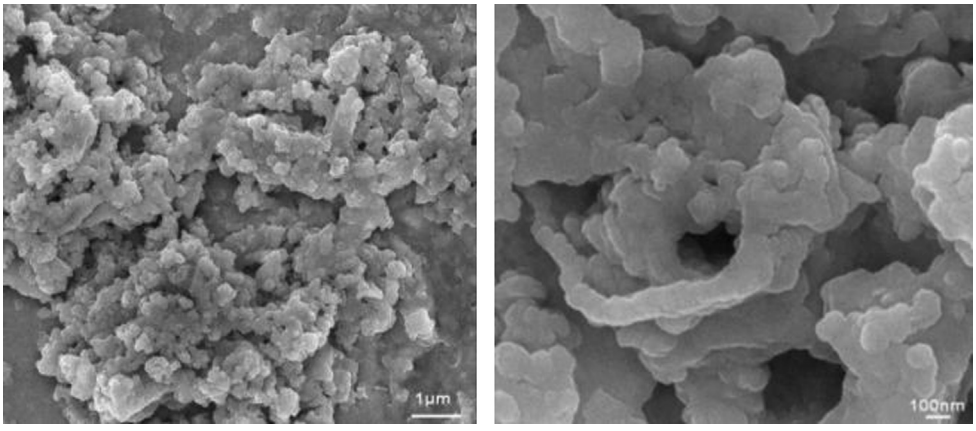

Fig. 3. Micrographs of ZrC powders.

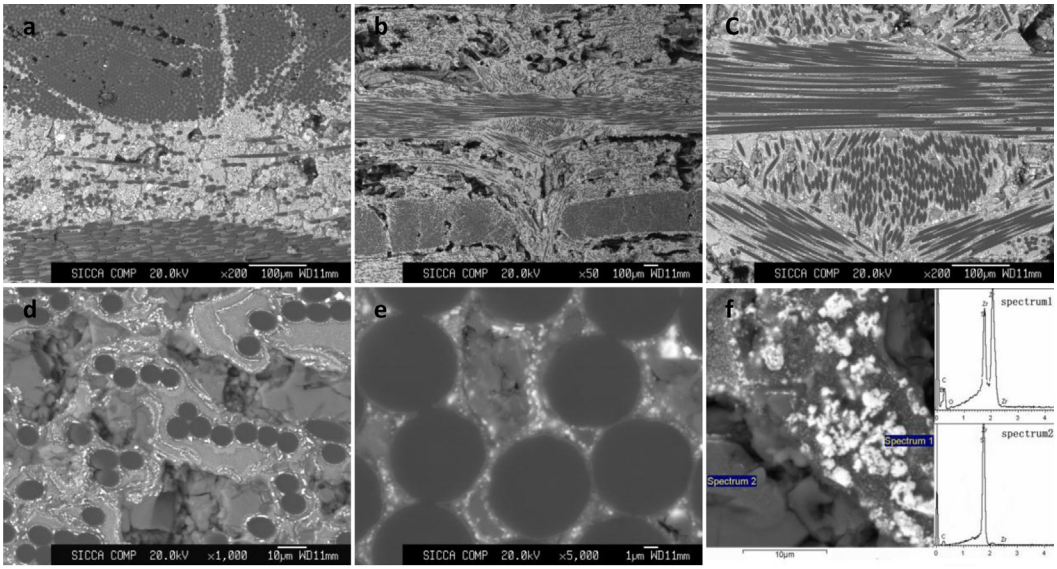

Fig. 4. Microstructure comparison of C/SiC–ZrC composites fabricated by different processes (a. composite S, b–f. composite S*).

zones. After several cycles PIP process, a great amount of PSZ-pyrolized-residues is present, which will convert into ZrC phases through carbothermal reduction reaction between ZrO_2 and carbon. The EDS analysis results (Fig. 4f) have confirmed the phases with bright contrast in composite S* to be ZrC and those with gray contrast to be SiC.

Some interesting phenomena can also be observed from the magnified graphs that ZrC phases formed in the matrix showed a layered structure, as shown in Fig. 4d and e. This may be ascribed to the unique densification process applied in this study, namely the preform was first impregnated with ZrC containing slurry, then PSZ was applied during first 6 PIP cycles while PCS was applied during the followed 6 PIP cycles. As mentioned above, in the slurry impregnation process, the voids between fiber filaments were mainly filled with ethanol and phenolic resin and the ethanol will vaporized in the drying process. Meanwhile, thanks to the excellent wetting ability of phenolic resin to carbon fiber, phenolic resin will adhere to the fiber surface. After pyrolysis, pyrolysed-carbon with lots of micro-pores will formed around the fibers. In the followed PIP process of PSZ, the residues will firstly formed in the micro-pores and around the outer surface of pyrolysed-carbon. Some pyrolysed-carbon will act as carbon sources and become gaseous CO during the carbothermal reduce reaction process. Due to the low ZrC yield of PSZ (about 30%–40%), the ZrC loading efficiency through PIP of PSZ is low. In the further densification process, with the application of high ceramic yield precursor, most of the pores will be filled with PCS-derived SiC. The differences in average atom weight as well as the matrix formation mechanism will account for the matrix with layered microstructure.

Some pulled-out fibers can be found in the fracture surface of composite S*, which will endow the composites with non-brittle fracture behavior and high reliability. Fig. 5(b, c) reveals that the length of pulled-out fibers has strong relevance to the direction of the fibers. Fibers in the 3D needle-punched preforms mainly arranged in three styles, namely 0° weftless carbon fibers, 90° weftless carbon fibers and randomly distributed short-cut fibers. In 3-point-bending testing process, 0° weftless carbon fibers which were normal to crack propagating direction as the samples were cut along the direction of 0° weftless fibers. Therefore, fiber pull-out will occur (Fig. 5b) when weak fiber/matrix interphases are designed. For 90° weftless carbon fibers, as they are parallel to the crack propagating direction, which mean they will not bear any load and contribute almost nothing to the strength. This is why no fiber pull-out will take place, only grooves can be observed (Fig. 5c). For short-cut webs, fiber pull-outs relate to the angle to the loading direction and small amount of short pulled-out fibers can be observed (Fig. 5d). Suemasu [19] confirmed the effect of the inclination of the fibers from the normal to the crack plane is extremely crucial for the short-fiber CMCs.

The mechanism for ablation resistance enhancement is also analyzed based on the microstructures of post-test composites on the testing surface. It can be concluded from the microstructures that there are some voids as well as craters on the exposed surface, as shown in Fig. 6a. The voids may be caused by the pores present in the short-cut fiber layers and the oxidation of carbon fibers. It can also observe that the craters mainly show bright contrast and some hollow with gray contrast can also be found among the craters (Fig. 6b). From the micrographs with

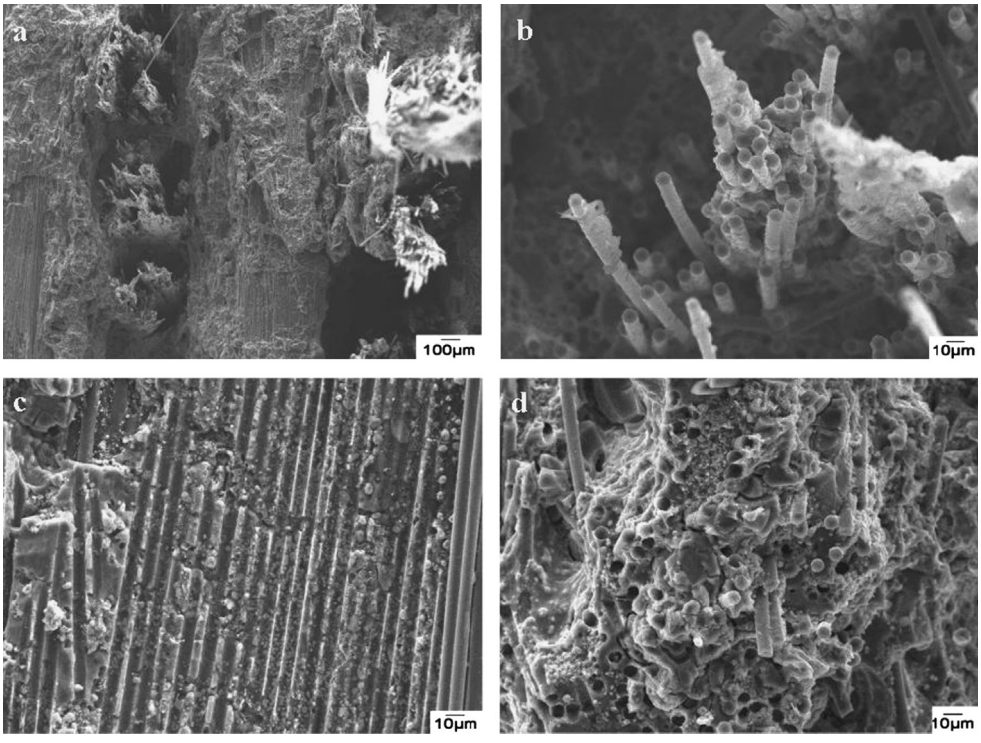

Fig. 5. SEM micrographs of C/SiC–ZrC composites on the facture surface.

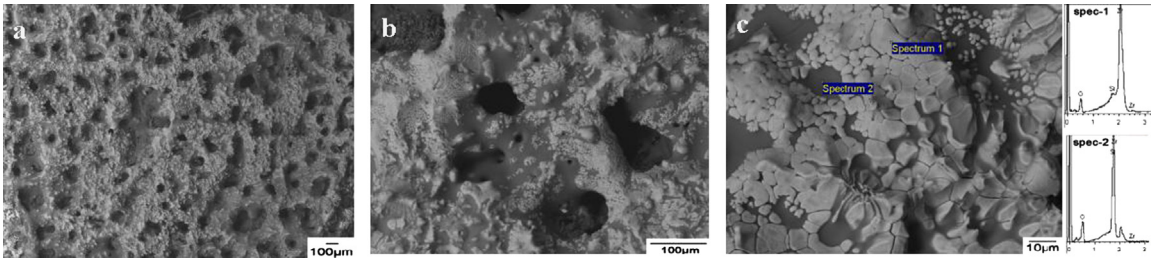

Fig. 6. SEM observation and EDS analysis on the exposed surface.

higher magnification (Fig. 6c), it can also find that there are lots of particles with the size of tens of micrometers and some particles tend to bond each other, but some particles are separated by phases with gray contrast. EDS analysis results indicated that phase with bright contrast was ZrO_2 and that with gray contrast was SiO_2. When the composites were exposed to high temperature gas, both SiC and ZrC will be oxidized by O_2 and dissociated oxygen [20]. In such high temperatures, the oxidation of SiC will take place mainly in form of active oxidation and form gaseous SiO. However, the oxidation of ZrC will lead to ZrO_2 and volume expansion will accompanied [21]. The volume shrinkage caused by loss of SiO and volume expansion caused by formation of ZrO_2 may account for hollows and craters on the exposed surface. As there is some difference in the distribution of ZrC in matrix, the amount of ZrO_2 formed is consequently different. The ultra high surface temperature on the exposed surface and the existence of SiO_2 fluid may account for the growth of ZrO_2 particles, meanwhile the formation of ZrO_2 scale may act as the main reason for ablation resistance enhancement of C/SiC–ZrC composites.

4. Conclusions

1. C/SiC–ZrC composites were fabricated via in-situ synthesis of ZrC using PSZ as a precursor. The amount and distribution homogeneity of ZrC in matrix can be greatly increased and SiC–ZrC matrix with layered structures can be observed from magnified graphs.
2. Some pulled-out fibers can be observed from the fracture surface, which means the deposited PyC/SiC interphases can protect carbon fibers from being eroded by ZrO_2 at high temperature.
3. The formation of ZrO_2 scale on the ablated surface as a result of oxidation of ZrC in matrix may amount for the enhanced ablation behavior of C/SiC–ZrC composites.

Acknowledgments

The authors acknowledge the financial support of this work by the National Natural Science Foundation of China under the Grant nos. 51002170 and 51172256 and Knowledge Innovation Program of Shanghai Institute of Ceramics Chinese Academy of Sciences under Grant no. Y12ZC6160G.

References

[1] F.Y. Yang, J.C. Han, S.Y. Du, Mechanical properties of short carbon fiber reinforced ZrB_2–SiC ceramic matrix composites, Materials Letters 62 (17–18) (2008) 2925–2927.
[2] F.Y Yang, J.C Han, S.Y. Du, Characterization of hot-pressed short carbon fiber reinforced ZrB_2–SiC ultra-high temperature ceramic composites, Journal of Alloys and Compounds 472 (1–2) (2009) 395–399.
[3] Z. Wang, S. Dong, X. Zhang, H. Zhou, D. Wu, Q. Zhou, D. Jiang, Fabrication and properties of C_f/SiC–ZrC composites, Journal of the American Ceramic Society 91 (10) (2008) 3434–3436.
[4] Z. Wang, S.M. Dong, Y.S. Ding, X.Y. Zhang, H.J. Zhou, J.S. Yang, B. Lu, Mechanical properties and microstructures of C_f/SiC–ZrC composites using T700SC carbon fibers as reinforcements, Ceramics International 37 (3) (2011) 695–700.
[5] H.B. Li, L.T. Zhang, L.F. Cheng, Y.G. Wang, Fabrication of 2D C/ZrC–SiC composite and its structural evolution under high-temperature treatment up to 1800 °C, Ceramics International 35 (7) (2009) 2831–2836.
[6] H. Hu, Q. Wang, Z. Chen, C. Zhang, Y. Zhang, J. Wang, Preparation and characterization of C/SiC–ZrB_2 composites by precursor infiltration and pyrolysis process, Ceramics International 36 (3) (2010) 1011–1016.
[7] L. Li, Y. Wang, L. Cheng, L. Zhang, Preparation and properties of 2D C/SiC–ZrB_2–TaC composites, Ceramics International 37 (3) (2011) 891–896.
[8] D. Zhao, C. Zhang, H. Hu, Y. Zhang, Preparation and characterization of three-dimensional carbon fiber reinforced zirconium carbide composite by precursor infiltration and pyrolysis process, Ceramics International 37 (7) (2011) 2089–2093.
[9] Q. Li, H. Zhou, S. Dong, Z. Wang, J. Yang, B. Wu, J. Hu, Fabrication and comparison of 3D C_f/ZrC–SiC composites using ZrC particles/polycarbosilane and ZrC precursor/polycarbosilane, Ceramics International 38 (6) (2012) 5271–5275.
[10] Q. Li, S. Dong, Z. Wang, P. He, H. Zhou, J. Yang, B. Wu, J. Hu, Fabrication and properties of 3-D C_f/SiC–ZrC composites, using ZrC precursor and polycarbosilane, Journal of the American Ceramic Society 95 (4) (2012) 1216–1219.
[11] Q. Li, H. Zhou, S. Dong, Z. Wang, P. He, J. Yang, B. Wu, J. Hu, Fabrication of a ZrC–SiC matrix for ceramic matrix composites and its properties, Ceramics International 38 (5) (2012) 4379–4384.
[12] Y. Wang, X. Zhu, L. Zhang, L. Cheng, C/C–SiC–ZrC composites fabricated by reactive melt infiltration with $Si_{0.87}Zr_{0.13}$ alloy, Ceramics International 38 (5) (2012) 4337–4343.
[13] L. Zou, N. Wali, J.-M. Yang, N.P. Bansal, D. Yan, Microstructural characterization of a C_f/ZrC composite manufactured by reactive melt infiltration, International Journal of Applied Ceramic Technology 8 (2) (2011) 329–341.
[14] L. Zou, N. Wali, J.-M. Yang, N.P. Bansal, Microstructural development of a C_f/ZrC composite manufactured by reactive melt infiltration, Journal of the European Ceramic Society 30 (6) (2010) 1527–1535.
[15] Y. Wang, X. Zhu, L. Zhang, L. Cheng, Reaction kinetics and ablation properties of C/C–ZrC composites fabricated by reactive melt infiltration, Ceramics International 37 (4) (2011) 1277–1283.
[16] J. Chen, Y. Wang, L. Cheng, L. Zhang, Thermal diffusivity of three-dimensional needled C/SiC–TaC composites, Ceramics International 37 (8) (2011) 3095–3099.

[17] A. Sayir, Carbon fiber reinforced hafnium carbide composite, Journal of Materials Science 39 (19) (2004) 5995–6003.
[18] X. Tao, W. Qiu, H. Li, T. Zhao, Synthesis of nanosized zirconium carbide from preceramic polymers by the facile one-pot reaction, Polymers for Advanced Technologies 21 (4) (2010) 300–304.
[19] H.K. Suemasu, A. Itatani, K. Nozue, A, A probabilistic approach to the toughening mechanism in short-fiber-reinforced ceramic–matrix composites, Composites Science and Technology 61 (2) (2001) 281–288.
[20] M. Tului, G. Marino, T. Valente, Plasma spray deposition of ultra high temperature ceramics, Surface and Coatings Technology 201 (5) (2006) 2103–2108.
[21] H. Zhou, L. Gao, Z. Wang, S. Dong, ZrB_2–SiC oxidation protective coating on C/C composites prepared by vapor silicon infiltration process, Journal of the American Ceramic Society 93 (4) (2010) 915–919.